

Validation of the multiscale mixed finite-element method

Mayur Pal^{1*}, Sadok Lamine², Knut-Andreas Lie³, and Stein Krogstad³

¹ *Maersk Oil and Gas, Denmark*

² *Shell Intl., Netherlands,*

³ *SINTEF ICT, P.O. Box 124, Blindern, N-0314 Oslo, Norway*

SUMMARY

Subsurface reservoirs generally have a complex description in terms of both geometry and geology. This poses a continuing challenge in modeling and simulation of petroleum reservoirs due to variations of static and dynamic properties at different length scales. Multiscale methods constitute a promising approach that enables efficient simulation of geological models while retaining a level of detail in heterogeneity that would not be possible via conventional upscaling methods.

Multiscale methods developed to solve coupled flow equations for reservoir simulation are based on a hierarchical strategy in which the pressure equation is solved on a coarsened grid and the transport equation is solved on the fine grid, and the two equations are treated as a decoupled system. In particular, the multiscale mixed finite-element (MsMFE) method attempts to capture sub-grid geological heterogeneity directly into the coarse-scale equations via a set of numerically computed basis functions. These basis functions are able to capture the predominant multiscale information and are coupled through a global formulation to provide good approximation of the subsurface flow solution.

In the literature, the general formulation of the MsMFE method for incompressible two-phase and compressible three-phase flow has mainly addressed problems with idealized flow physics. In this paper, we first outline a recent formulation that accounts for compressibility, gravity, and spatially-dependent rock-fluid parameters. Then, we validate the method by evaluating its computational efficiency and accuracy on a series of representative benchmark tests that have a high degree of realism with respect to flow physics, heterogeneity in the petrophysical models, and geometry/topology of the corner-point grids. In particular, the MsMFE method is validated and compared against an industry-standard fine-scale solver. The fine-scale flux, pressure, and saturation fields computed by the multiscale simulation show a noteworthy improvement in resolution and accuracy compared with coarse-scale models. Copyright © 2010 John Wiley & Sons, Ltd.

Received . . .

KEY WORDS: Multiscale methods; mimetic methods; basis functions; geological modeling; reservoir simulation; upscaling; fractures and barriers

1. INTRODUCTION

In the past few years, there has been an increasing interest in multiscale methods for a wide variety of engineering problems. The research in the area of multiscale methods is primarily motivated by the complexity and inherent multiscale nature of problems across a wide range of engineering disciplines, the rapid growth of computational power, and the need to solve highly detailed multiscale problems accurately and efficiently. For most engineering problems that involve a wide span of scales, it is often sufficient to accurately predict the macroscale behavior of

*Correspondence to: Maersk Oil and Gas, Esplanen 50, Copenhagen, Denmark. (This work was carried out while the author worked at Shell Intl.) E-mail: mayur.pal@maerskoil.com

Contract/grant sponsor: Publishing Arts Research Council; contract/grant number: 98–1846389

the system and it is not possible, or simply too expensive, to perform simulations that provide quantitative information about physical processes at all relevant scales, even with modern day computers. However, accounting for macroscopic effects only may not give the accuracy required because small-scale properties usually have a significant impact on the macroscale behavior. A popular approach to resolve this problem, is to assume scale separation, which means that one can define distinct characteristic scales for processes/effects that take place on the macroscopic scale and can be resolved on a computational grid, and processes/effects that take place locally on the subgrid scale. So-called multiscale methods [1, 2] are designed to accurately and effectively solve problems having multiple scales and offer a systematic framework for incorporating effects from an unresolved scale into the global flow equations in a manner that is consistent with the underlying differential operators. To accurately account for fine-scale effects in the macroscopic description, most multiscale methods rely on fine-scale computations that only use information within local regions to build effective parametrizations of the fine-scale behavior.

The flow of hydrocarbons in subsurface rock formations is an example of multiscale processes that do not have apparent scale separation. In many aspects, such problems are more challenging because nonlocal information is needed if one wants to compute effective properties that accurately represent subgrid effects. As a result, most existing multiscale methods rely on sophisticated combinations of fine-scale and coarse-scale computations to resolve the most important fine-scale information efficiently without having to compute directly on the global fine-scale problem. For petroleum reservoir simulation, in particular, multiscale methods are formulated so that fine-scale petrophysical and geological effects are captured directly in the coarse-scale simulation model without the need for explicit computation of effective properties.

Quite a number of such multiscale methods have been presented in the literature, including dual-grid methods [3, 4, 5, 6], finite-element methods [7], mixed finite-element [8, 9, 10, 11], and finite-volume methods [12, 13, 14, 15, 16, 17]. Apart from algorithmic differences, all of these methods share the same basic concept of incorporating fine-scale information into the coarse-scale equations via some sort of numerically constructed functions. These functions, also known as basis functions [7], contain fine-scale information embedded in the solution and are coupled through a global formulation to provide an accurate approximation of the flow solution. In a typical multiscale method, the pressure is first solved on a coarse grid and then propagated to a much finer grid using the basis functions. These basis functions can be computed locally, globally, or by using an adaptive-local global approach [11] to fill in the details of the fluxes that are required to subsequently compute the saturation change on the finer grid. In this two-grid approach, the pressure and saturation equations are decoupled. The pressure equation is solved on a coarse grid and a mass-conservative fine-scale flux field is recovered to solve the transport equation on the underlying fine grid. Most of the multiscale methods presented to date aim at capturing sub-scale pressure solutions with a predominantly elliptic nature.

Despite their obvious similarities, multiscale methods should not be confused with upscaling. A comprehensive comparison of multiscale methods with state-of-the-art upscaling methods for elliptic problems in porous media is presented in [18]. The main objective of the multiscale method is to efficiently obtain an accurate approximation to the fine-scale solution, whereas the intent of upscaling is to generate approximate coarse-scale solutions [19, 20]. Moreover, the natural coupling of local and global scales in multiscale methods reduces inconsistency and non-physical coarse-scale properties that are often associated with many upscaling techniques.

To date, there are almost no papers that validate multiscale methods on cases containing the complexity in geology and flow physics seen in real-life models used in industry. Herein, our main purpose is to present the result of such a validation study in which the multiscale mixed finite-element method is applied to simulate two-phase, incompressible flow on challenging and geologically realistic corner-point grids for cases including gravity and relative-permeability and capillary functions that vary with rock type. As part of the validation, the method is benchmarked against an industry-standard simulator. We also present preliminary test results for an idealized case of compressible two-phase flow described by the black-oil equations and discuss what we perceive as the main challenges in extending the method to more complex flow physics.

The multiscale formulations presented in this paper have been implemented in the open-source MATLAB Reservoir Simulation Toolbox (MRST) [21] which can be downloaded and freely used under the GNU General Public License (GPLv3). The numerical results presented in this paper are generated using functionality from the `msmfem` module in MRST.

This paper is organized as follows: the mathematical equations governing flow in porous medium are briefly reviewed in Section 2. Section 3 presents the basics of the multiscale mixed finite-element formulation and also outlines how to extend the method to incorporate compressibility, capillary, and gravity forces. Numerical results are presented in Section 4, followed by a summary and concluding remarks in Section 5.

2. MATHEMATICAL MODEL AND FINE-SCALE DISCRETIZATION

The partial differential equations governing two-phase incompressible flow in a porous medium can be derived from the continuity equation over an arbitrary domain Ω , given for phase i as follows:

$$\phi \frac{\partial S_i}{\partial t} + \nabla \cdot \vec{v}_i = q_i, \quad (1)$$

and Darcy's law describing relationship between the phase velocity \vec{v}_i and phase pressure p_i ,

$$\vec{v}_i = -\mathbf{K} \lambda_i (\nabla p_i - g \rho_i \nabla z). \quad (2)$$

Here, ϕ and \mathbf{K} denote porosity and permeability, which are both both represented in terms of constant values inside the cells of a space-filling, volumetric grid. Each phase i is described by a density ρ_i , a saturation S_i , a fluid source/sink q_i , and a phase mobility $\lambda_i = k_{ri}/\mu_i$, where μ_i denotes the viscosity and k_{ri} the relative permeability, i.e., the reduced permeability observed by one fluid phase in the presence of the other phase. Finally, g is the gravity constant and z the vertical coordinate. To obtain a solvable system, we need to define some closure relations. Herein, we only consider two phases, water (w) and oil (o), which are assumed to fill the pore volume so that $S_o + S_w \equiv 1$. Moreover, the two fluid pressures are related by the capillary pressure $p_c = p_o - p_w$, which is assumed to be given as a function of fluid saturation.

In an incompressible model, pressure signals propagate with an infinite speed whereas fluids are displaced by fronts that travel at a finite speed. To better represent these different physical characteristics, it is common to reformulate the model equations as one equation for pressure and one equation for transport. The pressure equation is elliptic while the transport equation is generally parabolic but has a strong hyperbolic character. To this end, we define the flow rate $q = q_o + q_w$ and introduce the total mobility $\lambda_t = \lambda_w + \lambda_o$, the fractional flow function $f_i = \lambda_i/\lambda_t$, and the total velocity $\vec{v}_t = \vec{v}_w + \vec{v}_o$. Then we can derive the following equation for oil pressure and total velocity,

$$\nabla \cdot \vec{v} = q, \quad \vec{v} = -\mathbf{K} \lambda [\nabla p_o - \tilde{g}(S_w) \nabla z + h(S_w) \nabla p_c], \quad (3)$$

and an evolution equation for the water saturation

$$\phi \frac{\partial S_w}{\partial t} + \nabla \cdot f_w(S_w) [\vec{v} + \mathbf{K} \lambda_o(S_w) ((\rho_w - \rho_o) g \nabla z + \nabla p_c(S_w))] = \frac{q_w}{\rho_w}. \quad (4)$$

Here, $\tilde{g}(S_w) = [f_w(S_w)\rho_w + f_o(S_w)\rho_o]g$ represents gravity effects and the form of the function $h(S_w)$ depends upon the choice of primary pressure variable; if we choose oil pressure, $h(S_w) = f_w(S_w)$. For simplicity, we will henceforth drop the subscripts on the primary variables p and S .

2.1. Pressure equation

To solve the system (3)–(4) numerically, the computational domain Ω is partitioned into a set of N non-overlapping polyhedral cells. Each cell C_i can have an arbitrary number of n_i planar faces, and each face matches the face of a neighboring cell. Let \mathbf{u}_i denote the vector of outward fluxes from

cell C_i , p_i denote the pressure at the cell center, and π_i the pressure at the cell faces. We then apply a standard, locally conservative discretization of Darcy's law

$$\mathbf{u}_i = \mathbf{T}_i [e_i p_i - \pi_i], \quad e_i = (1, \dots, 1)^T, \quad (5)$$

where \mathbf{T}_i is the matrix of one-sided transmissibilities. In the presence of gravity and capillary forces, the discretization takes the form,

$$\mathbf{u}_i = \mathbf{T}_i [e_i p_i - \pi_i - \tilde{g}(S_i) \Delta z_i + h(S_i) (e_i p_c(\vec{x}_i, S_i) - p_{ci})]. \quad (6)$$

Here, Δz_i denotes the vector of differences in the z -coordinate of the cell center \vec{x}_i and the face centroids. The capillary pressure p_{ci} at the cell faces is discretized using a standard two-point flux-approximation (TPFA) method.

By augmenting (6) with flux and pressure continuity across cell faces, we can derive the following discrete linear system for the global flow problem,

$$\begin{bmatrix} \mathbf{B} & \mathbf{C} & \mathbf{D} \\ \mathbf{C}^T & \mathbf{0} & \mathbf{0} \\ \mathbf{D}^T & \mathbf{0} & \mathbf{0} \end{bmatrix} \begin{bmatrix} \mathbf{u} \\ -\mathbf{p} \\ \boldsymbol{\pi} \end{bmatrix} = \begin{bmatrix} -\mathbf{G}(\mathbf{S}) \Delta \mathbf{z} + \mathbf{H}(\mathbf{S}) \Delta \mathbf{p}_c \\ \mathbf{q} \\ \mathbf{0} \end{bmatrix}. \quad (7)$$

Here, \mathbf{u} denotes the outward face fluxes ordered cell wise (fluxes over interior faces and faults appear twice with opposite signs), \mathbf{p} denotes the cell pressure, and $\boldsymbol{\pi}$ the face pressures.

To solve (7), we use a block-wise Gaussian elimination to give a positive definite system (the so-called Schur complement) for the face pressures

$$(\mathbf{D}^T \mathbf{B}^{-1} \mathbf{D} - \mathbf{F}^T \mathbf{L}^{-1} \mathbf{F}) \boldsymbol{\pi} = \mathbf{F}^T \mathbf{L}^{-1} \mathbf{q}, \quad (8)$$

where $\mathbf{F} = \mathbf{C}^T \mathbf{B}^{-1} \mathbf{D}$ and $\mathbf{L} = \mathbf{C}^T \mathbf{B}^{-1} \mathbf{C}$. Once the face pressures have been computed, the cell pressures and fluxes can be reconstructed by back-substitution,

$$\mathbf{L} \mathbf{p} = \mathbf{q} + \mathbf{F} \boldsymbol{\pi}, \quad \mathbf{B} \mathbf{u} = \mathbf{C} \mathbf{p} - \mathbf{D} \boldsymbol{\pi}.$$

The disadvantage of using the hybrid formulation (7) is that we get a linear system with significantly more degrees-of-freedom than for a straightforward cell-centered two-point scheme; the advantage is that the general form (7) includes consistent discretizations like multipoint and mimetic schemes, and as we shall see later, the multiscale mixed finite-element method. In terms of computational costs, we also notice that the Schur complement only involves \mathbf{B}^{-1} which can be constructed algebraically for many numerical schemes including, in particular, the standard two-point method, mimetic methods [22, 23, 24], and the MPFA-O method [25, 26, 27]. Moreover, the matrix \mathbf{L} is by construction diagonal and hence simple to invert.

2.2. Transport equation

The transport equation (4) is solved on the fine-scale grid using a standard discretization based on upstream-weighted mobilities. In the absence of gravity and capillary forces, the resulting scheme reads

$$S^{n+1} = S^n - \Delta t \mathbf{V}^{-1} \mathbf{U} \mathbf{F}(S^m) - \max(\mathbf{q}, 0) - \mathbf{f}(S^m) \min(\mathbf{q}, 0). \quad (9)$$

Here, \mathbf{V} is a diagonal matrix of pore volumes, while \mathbf{U} is a matrix with dimension equal the number of cells times the number of faces giving the flux contribution from Darcy fluxes for each face. Finally, \mathbf{F} denotes the upstream-weighted fractional flow evaluated per face and \mathbf{f} the fractional flow function evaluated per cell. The discretization may be explicit ($m = n$) or implicit ($m = n + 1$) and the numerical accuracy can (of course) be improved by using higher-order upwind schemes, like the wave-oriented multi-dimensional schemes [28, 29].

Gravity effects are added by using upstream weighting in a straightforward manner. Furthermore, we use two-point differences to compute the contributions from the gradient of the capillary pressure (∇p_c) on a face between two neighboring cells i, j .

$$\mathbf{K} \nabla p_c(S) \approx \mathbf{K}_h (p_c(S_i) - p_c(S_j)) / |\vec{c}_{ij}|, \quad (10)$$

where \vec{c}_{ij} is the centroid difference between cells i and j and \mathbf{K}_h denotes the harmonic average of the cell permeabilities in the direction of the face normal.

3. THE MULTISCALE MIXED FINITE-ELEMENT METHOD

The early concepts of mixed multiscale finite-element (MsMFE) methods for solving Poisson-type elliptic equations,

$$\nabla \cdot \vec{v} = f, \quad \vec{v} = -\lambda(x)\nabla p, \quad \text{in } \Omega, \quad (11)$$

were introduced in [8] for Cartesian grids, modified to give conservative discretizations in [9], and later extended to general polyhedral grids in e.g., [10, 11]. The basic idea of the MsMFE method is to construct a special approximation space, consisting of a set of coarse-scale basis functions with resolution H that satisfy a flow equation locally and hence are consistent with the differential operator at a finer resolution h . The basis functions are usually computed numerically within each element. Apart from that, the MsMFE method follows the same procedure as standard mixed finite-element methods to solve for the H -scale variables. Once the H -scale solution has been found, an approximate, but mass-conservative solution can be reconstructed on the h scale using the local resolution inherent in each basis function. In practice, the method is formulated using two hierarchically nested grids as shown in Figure 1, a fine-scale grid on which the rock and rock-fluid properties are given, and a coarse simulation grid to which we associate the degree-of-freedom used to solve the global flow problem. In the following, we will go through the various parts of the method in more detail.

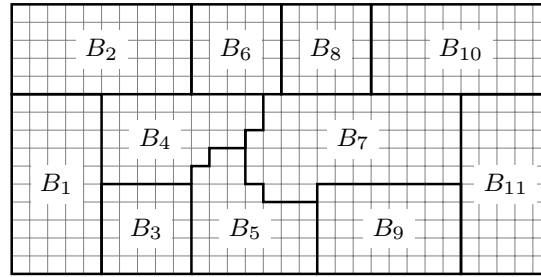


Figure 1. Illustration of the two-level grid used to define the MsMFE method. The coarse grid (thick lines) is formed based on a partition of the fine grid (thin lines) so that each coarse block B_j consists of a connected set of cells from the fine grid. Each block can, in principle, have arbitrary shape, but the best numerical accuracy is obtained if the blocks are somewhat regular, follow the layered structures of stratigraphic grids [10], and/or adapt to high-contrast features [30, 31].

3.1. Multiscale approximation

To formally define the MsMFE method, we start by writing the solution to (7) as the sum of the basis functions plus a fine-scale residual,

$$\mathbf{u} = \Psi \mathbf{u}_c + \tilde{\mathbf{u}}, \quad \mathbf{p} = \Phi \mathbf{p}_c + \tilde{\mathbf{p}}, \quad \boldsymbol{\pi} = \Pi \boldsymbol{\pi}_c + \tilde{\boldsymbol{\pi}}. \quad (12)$$

Here, \mathbf{u}_c denotes the vector of outward fluxes over the coarse-block interfaces, \mathbf{p}_c denotes the vector of coarse-block pressures, and $\boldsymbol{\pi}$ denotes the vector of coarse-block face pressures. Likewise, $\tilde{\mathbf{u}}$, $\tilde{\mathbf{p}}$, $\tilde{\boldsymbol{\pi}}$ are reminder terms having variations on the fine grid. The matrices Ψ , Φ , and Π represent the fine-scale reconstruction operators for \vec{v} , p , and π . Each column in Ψ corresponds to a multiscale basis function for the flux associated with a unique coarse-grid face and is represented as a $n_f \times 1$ vector of fine-scale fluxes.

For compressible flow, we also need to define fine-scale variations for the pressure basis so that each column of Φ is a basis function associated with a unique block and each column of Π corresponds to a basis function defined over a coarse face. For incompressible flow, on the other hand, pressure is seldom used explicitly except to determine well-rates through the use of appropriate well models. Hence, we define the pressure to be constant within each coarse block and replace Φ by a simple prolongation operator \mathbf{I} that maps a constant value from each coarse block onto the cells of the block. Likewise, Π is replaced by a prolongation operator \mathbf{J} that maps a

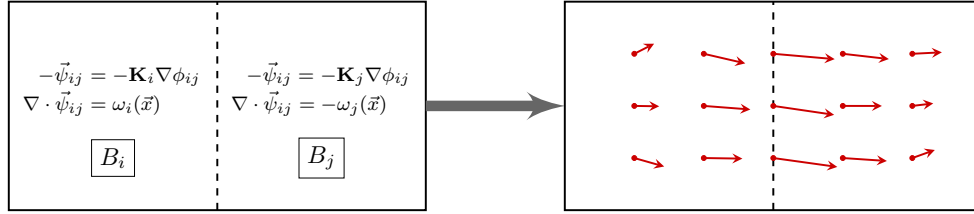


Figure 2. Illustration of the generation of a two-block basis function for the associated with the coarse flux across the interface Γ_{ij} between two coarse blocks B_i and B_j . Here, the blocks are rectangular, but the exact same construction applies to general polygonal/polyhedral blocks.

constant value from each coarse face onto the individual cell faces of the coarse face. Altogether, this defines a reconstruction operator $\mathbf{R} = \text{diag}(\Psi, \mathbf{I}, \mathbf{J})$ that enables us to map the degrees-of-freedom $\mathbf{x}_c = [\mathbf{u}_c, -\mathbf{p}_c, \boldsymbol{\pi}_c]$ on the coarse-scale to the corresponding fine-scale quantities $\mathbf{x} = [\mathbf{u}, -\mathbf{p}, \boldsymbol{\pi}]$.

3.2. Coarse system

To form a global system on the coarse grid, we need a compression operator that will bring the fine-scale system (7) to the space spanned by our multiscale basis functions. Here, \mathbf{R}^T is a natural choice since the transposed of the prolongation operators \mathbf{I} and \mathbf{J} correspond to the sum over all fine cells of a coarse block and all fine-cell faces that are part of the faces of the coarse blocks, respectively. Multiplying (7) from the left by \mathbf{R}^T , substituting $\mathbf{x} = \mathbf{R}\mathbf{x}_c$, and rearranging terms, we obtain

$$\begin{bmatrix} \Psi^T B \Psi & \Psi^T C I & \Psi^T D J \\ I^T C^T \Psi & 0 & 0 \\ J^T D^T \Psi & 0 & 0 \end{bmatrix} \begin{bmatrix} \mathbf{u}_c \\ -\mathbf{p}_c \\ \boldsymbol{\pi}_c \end{bmatrix} = \begin{bmatrix} \Psi^T (H(S)\Delta \mathbf{p}_c - G(S)\Delta \mathbf{z}) \\ I^T \mathbf{q} \\ \mathbf{0} \end{bmatrix}. \quad (13)$$

On the right-hand side, the fine-scale reminder terms were eliminated as follows: $\tilde{\mathbf{p}}$ disappears if we interpret the coarse-scale pressure as the w -weighted average of the true pressure, $p_c^i = \int_{B_i} w p d\vec{x}$, where w is the source term used to define basis functions, see Section 3.3. The two other terms, $\tilde{\mathbf{u}}$ and $\tilde{\boldsymbol{\pi}}$, are simply neglected. The coarse system (13) is on the same hybrid form as the fine-scale system (7) and can be solved using the Schur-complement reduction discussed in Section 2.1.

3.3. Multiscale basis functions

The basis function associated with a flux between two coarse blocks is constructed as illustrated in Figure 2. The resulting method is not convergent, but will typically give reasonable accuracy on finite grids. The purpose of the weight function $w_{ij}(\vec{x})$ is to distribute $\nabla \cdot \vec{v}$ over the coarse block. To ensure a unit flow across the interface Γ_{ij} , the weight function should be chosen on the form $w_i(\mathbf{x}) = \theta(\mathbf{x}) / \int_{B_i} \theta(\mathbf{x}) d\mathbf{x}$. The function $\theta(\mathbf{x})$ can be defined in several ways [32, 33]. For incompressible flow, the simplest choice is to set $\theta(\vec{x}) \equiv 1$ or $\theta(\vec{x}) = \text{trace}(\mathbf{K})$ away from the possible wells and $\theta(\vec{x}) = q(\vec{x})$ in grid blocks penetrated by wells. This will reproduce the lowest-order Raviart–Thomas basis on rectangular blocks with homogeneous, isotropic permeability. For incompressible flow, the pressure is immaterial and ϕ_{ij} can be replaced by a constant inside each block.

3.4. Capillary forces

To account for capillary forces, we introduce an additional set of basis functions defined as

$$\vec{\psi}_{ij}^p = -\mathbf{K}(\nabla \phi_{ij}^c - h(S)\nabla p_c(S)), \quad \nabla \cdot \vec{\psi}_{ij}^c = 0, \quad (14)$$

so that there are two flux bases associated with each coarse face. The new basis functions are included in the multiscale expansion (12) and in the coarse-scale system (13) by adding each

discrete approximation to $\vec{\psi}_{ij}^p$ as an extra column in Ψ . In other words, Ψ^0 denotes the basis functions defined in Section 3.3 and \mathbf{u}_c^0 the corresponding degrees of freedom, then $\mathbf{u}_c = [\mathbf{u}_c^0 \mathbf{u}_c^p]$ and $\mathbf{u}_c = [\mathbf{u}_c^0 \mathbf{u}_c^p]$.

Using an extra set of basis functions instead of adding capillary effects directly in the basis functions $\vec{\psi}_{ij}$ has the advantage that we avoid the problem of having to scale the relative contributions of the physical capillary terms and the artificial source term w_{ij} . It also reduces the saturation dependence in our set of basis functions.

3.5. Compressibility

The basic flow model (3) can be extended to compressible flow as follows

$$\nabla \cdot \vec{v} = q - c_t \frac{\partial p}{\partial t} + (\gamma(S, p) \vec{v} + \beta(p) \mathbf{K} g \nabla z) \cdot \nabla p, \quad \vec{v} = -\lambda \mathbf{K} (\nabla p - \tilde{g}(S) \nabla z), \quad (15)$$

where c_t denotes total compressibilities and $\beta(p)$ and $\gamma(S, p)$ are known functions of pressure- and saturation-dependent parameters. For simplicity, we neglect capillary forces and write the linearized discrete system on mixed form

$$\begin{bmatrix} \mathbf{B}^n & \mathbf{C} \\ \mathbf{C}^T & \mathbf{P}^n(\mathbf{p}_{\nu+1}^{n+1}) \end{bmatrix} \begin{bmatrix} \mathbf{v}_{\nu+1}^{n+1} \\ -\mathbf{p}_{\nu+1}^{n+1} \end{bmatrix} = \begin{bmatrix} \mathbf{f}^n(\mathbf{p}_{\nu}^{n+1}) \\ \mathbf{g}^n(\mathbf{p}^n, \mathbf{p}_{\nu}^{n+1}) \end{bmatrix}. \quad (16)$$

Here, ν indicates iterations in a nonlinear solver and superscript n indicates functional dependence on saturation/pressure from the previous time step; this superscript will be dropped for brevity.

MsmFE methods for systems on the form (16) have been discussed in detail in [34, 33]. For compressible flow, the pressure is no longer immaterial and ϕ_{ij} should thus include subscale pressure variations. To ensure that pressure and flux bases scale similarly, we use a saturation-dependent decomposition for pressure, $\mathbf{p} = \mathbf{I} \mathbf{p}_c + \mathbf{\Lambda} \Phi \mathbf{v}_c + \hat{\mathbf{p}}$, where $\mathbf{\Lambda} = \text{diag}(\lambda_\ell^0 / \lambda_\ell)$ and λ_ℓ^0 is the mobility used to calculate basis function ℓ . This gives the coarse-scale system

$$\begin{bmatrix} \Psi^T \mathbf{B} \Psi & \Psi^T \mathbf{C} \mathbf{I} \\ \mathbf{I}^T (\mathbf{C}^T \Psi - \mathbf{P}_\nu \mathbf{\Lambda} \Phi) & \mathbf{I}^T \mathbf{P}_\nu \mathbf{I} \end{bmatrix} \begin{bmatrix} \mathbf{v}_c^{\nu+1} \\ -\mathbf{p}_c^{\nu+1} \end{bmatrix} = \begin{bmatrix} \Psi^T \mathbf{f}_\nu \\ \mathbf{I}^T \mathbf{g}_\nu \end{bmatrix}, \quad (17)$$

which needs to be solved iteratively to construct a multiscale approximation. To get a fine-scale approximation that converges to zero fine-scale residual, we need to include an equation for the residual terms that were neglected in (17)

$$\begin{bmatrix} \mathbf{B} & \mathbf{C} \\ \mathbf{C}^T & \mathbf{P} \end{bmatrix} \begin{bmatrix} \hat{\mathbf{v}}^{\nu+1} \\ -\hat{\mathbf{p}}^{\nu+1} \end{bmatrix} = \begin{bmatrix} \mathbf{f}_c - \Psi^T \mathbf{B} \Psi \mathbf{v}_c + \Psi^T \mathbf{C} \mathbf{I} \mathbf{p}_c \\ \mathbf{g}_c - \mathbf{I}^T (\mathbf{C}^T \Psi - \mathbf{P}_\nu \mathbf{\Lambda} \Phi) \mathbf{v}_c + \mathbf{I}^T \mathbf{P}_\nu \mathbf{I} \mathbf{p}_c \end{bmatrix}. \quad (18)$$

If the residuals have a localized structure, this equation can be solved efficiently by a standard overlapping Schwarz method. Hence, the resulting iterative method, iMsmFE for short, consists of an outer loop, in which we iterate over (17) and (18) to reduce the fine-scale residual, and two inner loops that are used to solve (17) and (18), respectively.

4. NUMERICAL RESULTS

In this section, we will validate the MsmFE method on five different test cases with realistic reservoir geometries and petrophysical properties, as well as on models with spatially dependent fluid properties. The aim of the first test case is to assess the computational efficiency of the method on a large-scale geological model with approximately 700,000 cells. The second test case compares the performance of the multiscale method with the Shell standard simulator [35]. Case three and four aim to validate the multiscale method for incompressible two-phase flow with gravity and spatially-dependent rock-fluid parameters. Case three involves two regions with different relative

permeability and capillary curves, whereas the fourth case corresponds to a sector model with multiple rock types, with a different relative permeability and capillary curve associated with each rock type. The final test case demonstrates the use of MsMFE for compressible two-phase flow described by the black-oil equations.

To perform the numerical experiments, the MsMFE methods described above have been implemented as software prototypes in Matlab, using the Matlab Reservoir Simulation Toolbox (MRST) [36]; all examples except for the fifth were computed with functions that are publicly available in the `msmfem` module in MRST Release 2011b [21] and later. The main purpose of MRST is to simplify the prototyping and testing of new computational methods on general unstructured grids. This means that computational efficiency has been sacrificed in certain cases for the sake of generality and flexibility of the toolbox. In particular, the data structure used to represent basis functions in the `msmfem` module introduces significant computational overhead when extracting basis functions to assemble coarse systems. To get a more reliable assessment of the computational efficiency of the MsMFE method, we have developed a C-accelerated version of the incompressible method, in which all steps except for the linear solver of the coarse system are performed in C via a MEX interface to Matlab. Moreover, in both the C-accelerated and the pure Matlab versions, the basis functions are, for the sake of generality, implemented using a mimetic discretization with a two-point type inner-product (see [36]), which is a factor 3–10 less efficient than using a standard cell-centered TPFA implementation. The computational performance of the MsMFE method is therefore expected to be at least a factor 3–5 times better if the method is implemented using a (tailor-made) cell-centered fine-scale discretization.

All computational experiments reported in the following refer to simulations performed on a computer with Intel Core2 Duo Processors (6M Cache, 2.80 GHz, 1066 MHz FSB) and 4 GiB RAM.

4.1. Example 1: large geomodel

In the first test case, we evaluate the efficiency of the MsMFE solver implemented in MRST and, in particular, compare the C-accelerated version to its pure Matlab counterpart. To this end, we consider a realistic large-scale geomodel shown in Figure 3. The simulation grid is given as a corner-point grid with $253 \times 258 \times 38$ cells. After cells with zero porosity or permeability are set to be inactive, the total simulation model consists of 721,999 active cells. In addition, we have introduced a lower permeability threshold of $1 \mu\text{D}$. We consider a scenario in which water is injected into a reservoir that is initially fully oil saturated. The system is described by a standard two-phase model with a mobility ratio ten between the two fluids. In our timing experiments, we will focus exclusively on the pressure equation and not consider the transport solves that would normally have been performed on the fine scale. Our simulation setup consists of first computing basis functions, and then solving the global pressure equation one thousand times.

For multiphase flow applications, the basis functions are generally time-dependent and coupled to the transport equation through the relative mobility term λ . For water-flooding scenarios, however, this temporal dependence is typically quite weak and good multiscale solutions can be computed using infrequent updating of basis functions. Thinking of a BuckleyLeverett type displacement profile, $\lambda(\mathbf{x}, t)$ will typically only vary modestly before and after the block is swept by the displacement front. Favorable displacements will typically contain strong displacement fronts, and here individual basis functions need to be updated frequently to account for large mobility variations as the front passes through the interior of the corresponding blocks. For unfavorable displacements, as considered herein, it is often sufficient to only compute the basis functions initially [18]. To mimic a worst-case scenario of mobility effects arising from saturation updates, the pressure system is reinitialized by assigning random relative permeability values to all cells before each new pressure solve. By updating the pressure one thousand times, we get a picture of where the time is spent during a dynamic simulation. For instance, given a pressure step of ten days, our test will mimic a simulation of 27 years of production.

First we compare time consumption on a subset of the full geomodel. The results are displayed in Table I. The C-accelerated code gives a reduction in runtime of over 80% compared to the pure

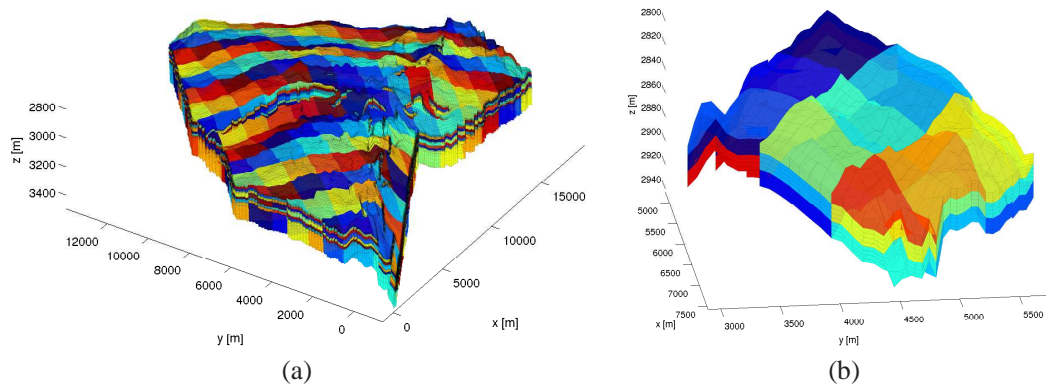


Figure 3. The geomodel. The plot in (a) shows the full $253 \times 258 \times 38$ model with a $15 \times 15 \times 7$ coarse grid imposed. The plot in (b) shows a subset of the full model.

MATLAB implementation even though the MEX interface is not optimal since data must be copied between C and MATLAB. Solving the same system on the fine scale with the AGMG multigrid solver [37] takes 200 seconds, and hence the MsMFE solver gives a reduction of 86% in runtime compared to the fine-scale solver for the pure Matlab solver and 97% for the C-accelerated solver.

The results for the C-accelerated code on the full geomodel are shown in Table II. For large data sets, as in this case, implementing the whole multiscale simulator in a compiled language would be much more efficient, since a significant computational overhead is induced when using the MEX interface to copy data between MATLAB and C in the C-accelerated MRST code. In particular, for the reconstruction of fine-scale fluxes, which is the most expensive operation reported in Table II, over 50% of the time is spent copying data. Moreover, an obvious advantage of the MsMFE solver is that it has a relatively low memory use compared e.g., with the AGMG solver, which required more memory than the 4 GiB that were available on our meager test computer. Finally, in the simulations reported above, the basis functions were computed serially. Since each basis function can be computed independently of the other, this part of the algorithm is straightforward to parallelize and is expected to give an almost perfect speedup. Parallelizing the reconstruction of fine fluxes is a bit more complex, but should also give a significant speedup.

We expect that the results presented above extend readily to *incompressible* black-oil models in the absence of gravity and capillary forces: the key to efficiency is to reuse basis functions from one step to the next and exploit the natural parallelism in computing basis functions and reconstructing fine-scale fluxes.

4.2. Example 2: Carbonate sector model

The geometrical and physical properties used in this particular sector model are based on a real-field carbonate reservoir. The sector model covers a 2×2 km² area and has a thickness of approximately fifty meters. The fine-scale model has 20×20 cells in the lateral direction and 93 cell layers in the vertical direction, which we partition into a coarse grid with $5 \times 5 \times 11$ blocks. For comparison, we also generate a corresponding upscaled model based on a standard flow-based method. Figure 4 shows the fine-scale porosity distribution, the coarse partition used by the multiscale method, as well as the upscaled model. Here, we see that unlike the upscaling method, the multiscale partition preserves the exact geometry of the fine-scale model.

The reservoir is produced using a five-spot injection pattern, with one injector at each corner of the model and one producer in the center. The fluid and the reservoir data used for the simulations are presented in Table III. The model represents a scenario with 2000 days of production.

In the following, we will compare four different simulation strategies: using standard sequential solvers from MRST on the coarse and fine grids, using the MsMFE method, and using Shell's

Table I. Runtimes in seconds for one thousand pressure updates for a $20 \times 20 \times 12$ subset of the full geomodel with a $3 \times 3 \times 3$ coarse grid. Fine-scale solution with AGMG: 200.07 seconds.

Task	C-accelerated		pure Matlab	
	time [sec]	% of total	time [sec]	% of total
Construct coarse grid (x1)	0.01	0.08	0.02	0.07
Compute basis functions (x1)	0.74	14.53	1.68	6.05
Assemble coarse system (x1000)	0.94	18.37	20.09	72.20
Solve coarse system (x1000)	1.81	35.14	1.92	6.90
Reconstruct fine flux (x1000)	1.64	31.86	4.11	14.76
Total time	5.14	100.00	27.82	100.00
Reduction compared to AGMG	97%		86%	

Table II. Time consumption in seconds for the full $253 \times 258 \times 38$ geomodel with 1000 pressure steps, for C-accelerated multiscale code without updating the basis functions.

Task	$10 \times 10 \times 5$		$15 \times 15 \times 7$	
	time [sec]	% of total	time [sec]	% of total
Construct coarse grid (x1)	0.09	0.01	0.01	0.01
Compute basis functions (x1)	323.42	40.48	224.24	31.33
Assemble coarse system (x1000)	46.46	5.82	54.69	7.64
Solve coarse system (x1000)	25.35	3.17	54.12	7.56
Reconstruct fine flux (x1000)	403.62	50.52	382.61	53.46
Total time	798.95	100.00	715.76	100.00

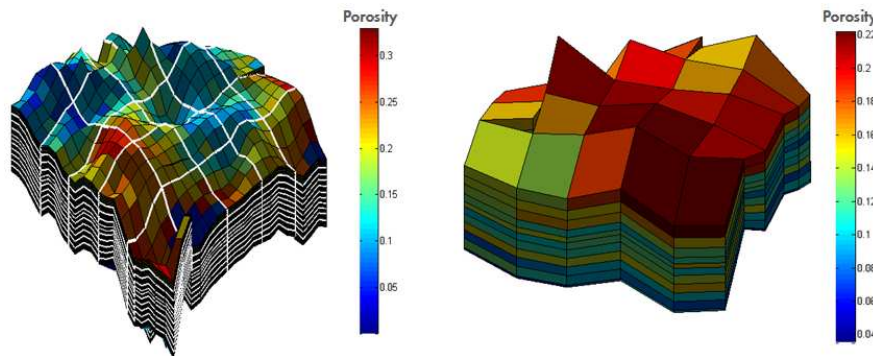


Figure 4. Sector model of a carbonate reservoir. The left plot shows the porosity with white lines indicating the $5 \times 5 \times 11$ coarse partition. The right plot shows the upscaled version of the same model.

Table III. Fluid and reservoir data used for the sector model

Property	Value	Unit
Water viscosity	0.393	cP
Oil viscosity	1.1	cP
Water density	1138	Kg/m ³
Oil density	832	Kg/m ³
Connate water saturation	0.2	—
Irreducible oil saturation	0.2	—
Initial reservoir pressure	6000	psi
Well injection rate	10000	bbl/day

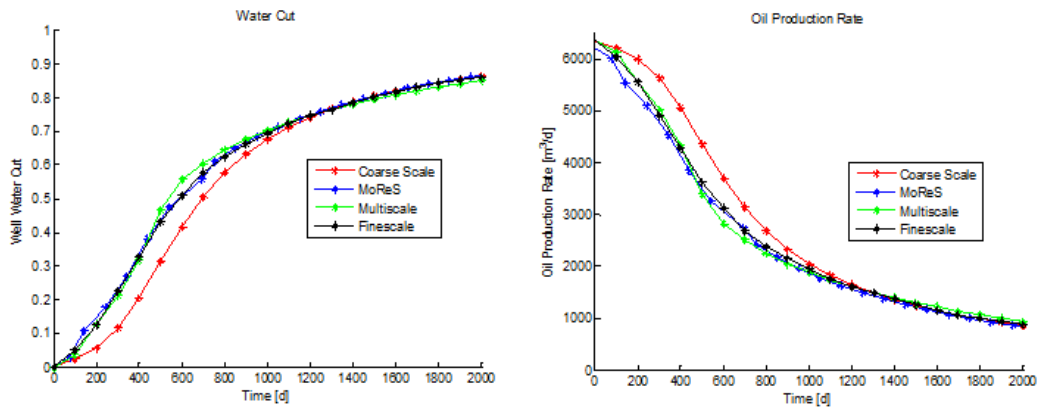


Figure 5. Water cut and oil production curves for the carbonate sector model.

simulator MoReS [35] on the fine grid. Figure 5 reports the resulting water-cut and oil-production curves. The production curves predicted by MoReS and the MRST fine-scale solver coincide more or less. The MsMFE solver is in close agreement with the two fine-scale simulations, except for a slightly higher water cut between days 500 and 700, which is compensated by a slightly lower water cut towards the end of the production period. The upscaled simulation gives a significant overprediction of oil rate and underprediction of water rate during the first twelve hundred days.

Figure 6 shows the corresponding saturation profiles computed in the four different simulations. The coarse model predicts significantly different results than the other three simulations, and would not have been used for simulation in practice. On the other hand, the cost of updating the pressure is almost the same for the upscaled and the multiscale simulation, and the coarse-scale saturation profiles have been included to demonstrate what can be gained by exploiting the subresolution that is inherent in the multiscale basis functions to compute saturations. However, the most interesting comparison is between the fine-scale MoReS and the multiscale/fine-scale MRST simulations. Clearly, the standard sequential solver in MRST produces almost identical results as MoReS on the same grid. Moreover, the volumetric sweep predicted by the multiscale simulation is in close agreement with the two fine-scale simulations.

4.3. Example 3: Box model with two rock types

The previous example validated the fine-scale and multiscale MRST solvers against Shell’s in-house reservoir simulator for a sector model with realistic heterogeneity and geometry, but with simplified flow physics. In the next example, we will consider more realistic flow physics that includes gravity and spatially-dependent rock-fluid properties. To this end, we will use a simple 2D box that consists of two different rock types (saturation regions) that have different relative-permeability and capillary curves. The permeability of the medium is equal 100 milli darcy throughout the whole domain, and the porosity is homogeneous and equal 0.3. The reservoir is initially fully saturated with oil and is represented on a regular Cartesian grid with 20×20 cells, which we have partitioned uniformly into 5×5 coarse blocks, see Figure 7. Water is injected at the rate of $0.5 \text{ m}^3/\text{day}$ from the bottom of the domain and oil is produced from the top. Gravity is acting in the z -direction. The transport loop runs with a pressure step of 0.1 year. The initial fine-scale and multiscale pressure distributions are shown in Figure 7.

Figure 8 compares production curves and the evolution of the saturation profiles computed by the fine-scale and multiscale simulations. Because of the different capillary curves, the saturation profile of the injected water will be significantly different in the upper and lower parts of the domain. Despite that there are some differences in the saturation fields predicted by the multiscale and the fine-scale solver, the multiscale solver is able to predict the production curve with high accuracy, which in many workflows is the main purpose of using a flow simulation.

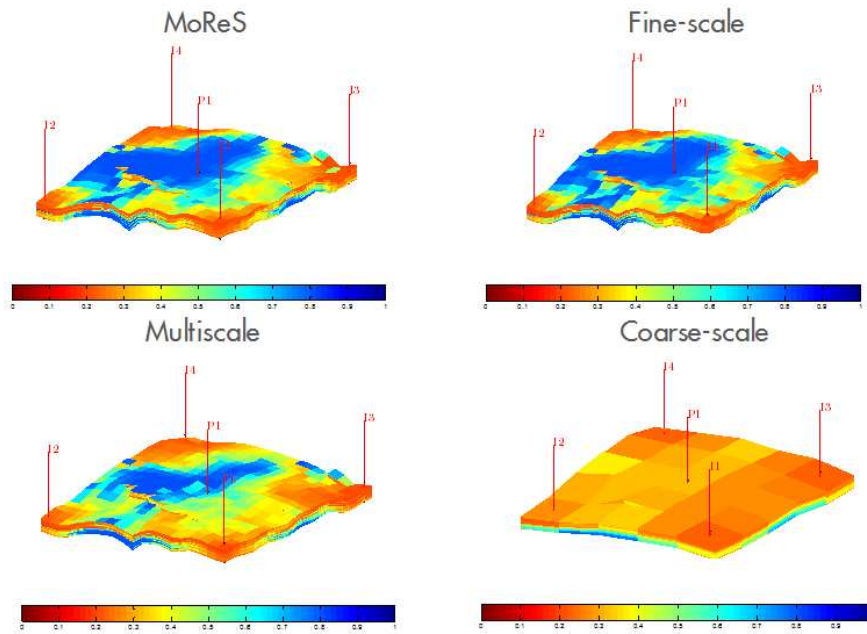


Figure 6. Saturation profiles for the carbonate sector model.

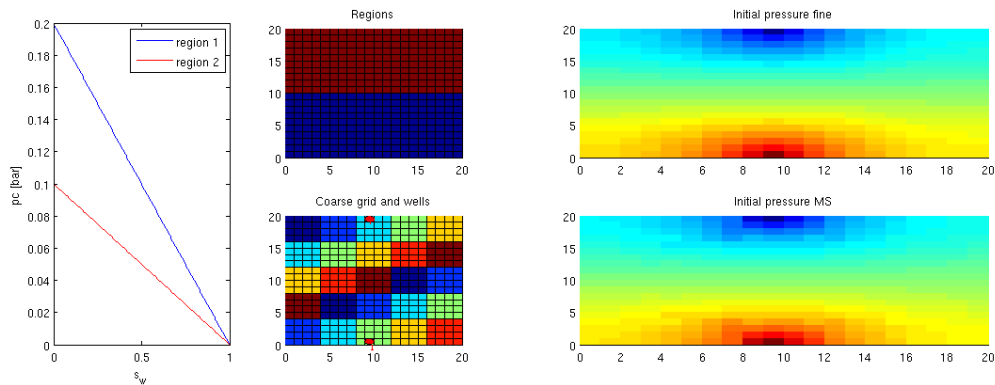


Figure 7. The plot to the left shows two different linear capillary curves corresponding to the two different rock types shown in the upper-middle plot. The lower-middle plot shows the placement of the injection and production wells and subdivision into coarse blocks. The plots to the right show the initial pressure distribution computed by the fine-scale and the multiscale solver.

4.4. Example 4: Sector model with nine rock types

We consider a $21 \times 21 \times 13$ sector model that covers an area of $3 \times 3 \text{ km}^2$ and has a thickness of approximately 100 m. The model contains nine different rock types that each has its own relative permeability and capillary curves, shown in Figure 9. Petrophysical data and well placement are presented in Figure 10. Initial reservoir pressure is 4728.23 psi and the reservoir is produced by two wells that are located at diagonally opposite corners of the model in a quarter five-spot pattern. The injection well operates at a rate constraint of 3000 STB per day. The production well operates at a bottom-hole pressure constraint of 100 psi.

Figure 11 shows the water saturation after twenty years and clearly demonstrates how the variation in capillary and relative permeability curves throughout the reservoir gives rise to

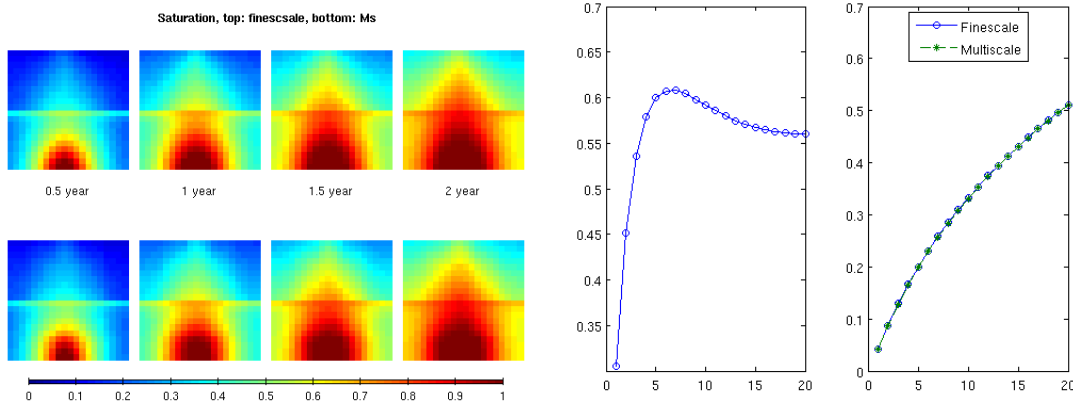


Figure 8. The plots to the left show saturation profiles for the fine-scale and multiscale simulation for the box model; capillary effects are clearly visible in the saturation distribution. The graph to the far right shows the water saturation in the production well as function of time computed by the fine-scale and the multiscale simulations. The graph in the middle shows the discrepancy in percent between the predicted saturation fields as function of time.

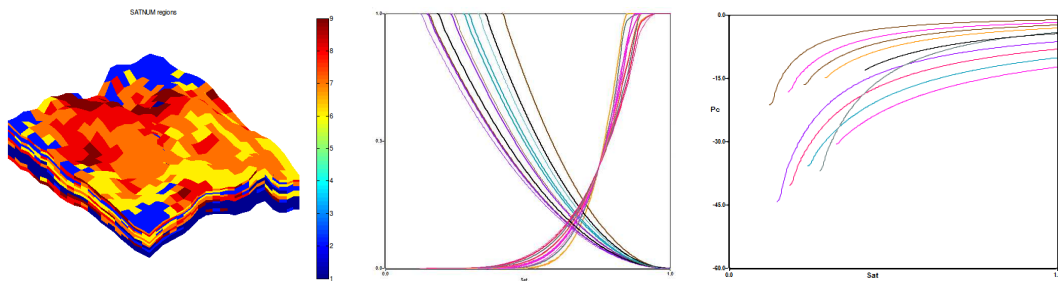


Figure 9. Sector model with nine different rock types. The left plot shows cells colored by the rock type (saturation region number). The middle and left plots show the corresponding relative permeability and capillary pressure curves, respectively.

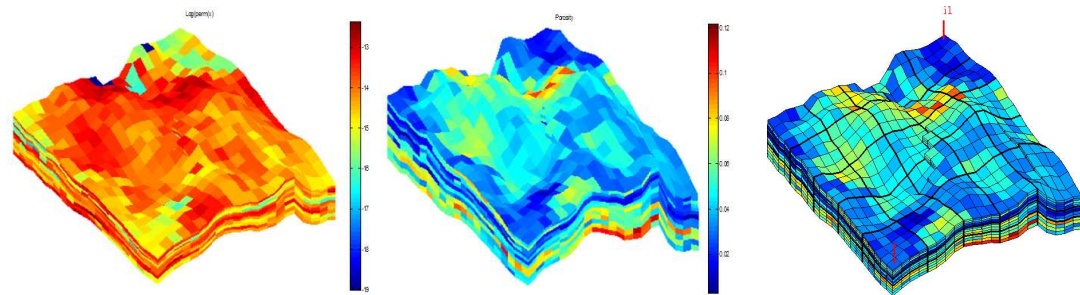


Figure 10. Petrophysical data for the $21 \times 21 \times 13$ sector model. The left plot shows the permeability, which spans the interval from 50 mD to 400 mD, and the middle plot shows the porosity, which varies in the interval $[0.02, 0.12]$. The right plot shows the well placement and a $5 \times 5 \times 3$ coarse grid, outlined on top of the original geo-cellular model.

significant heterogeneity effects. Figure 12 reports a more detailed analysis of the difference in the solutions computed by the fine-scale solver and the MsMFE solver operating on a $5 \times 5 \times 3$ coarse grid. Overall, the multiscale solver is able to predict the qualitative effects that gravity and spatial variations in the rock-fluid parameters have on the fine-scale flow patterns with reasonable accuracy. On the other hand, there are large pointwise discrepancies between the fine-scale and

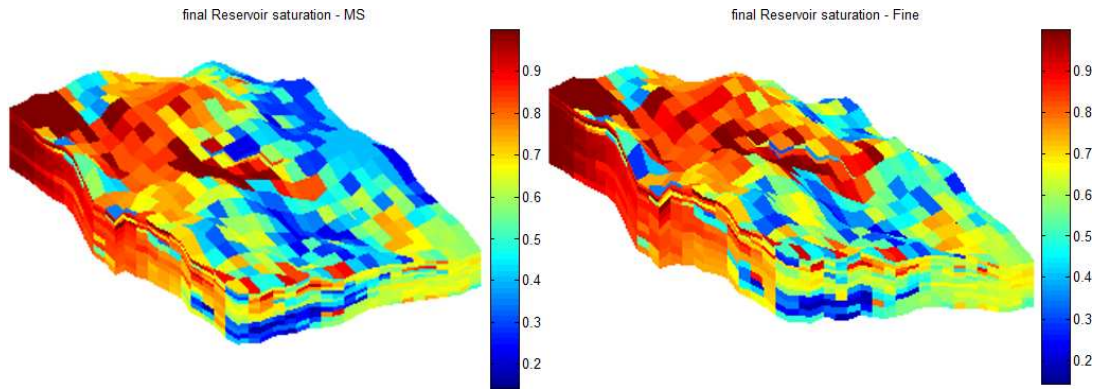


Figure 11. Water saturation distribution in the sector model after twenty years computed by the fine-scale solver (left) and the multiscale solver (right).

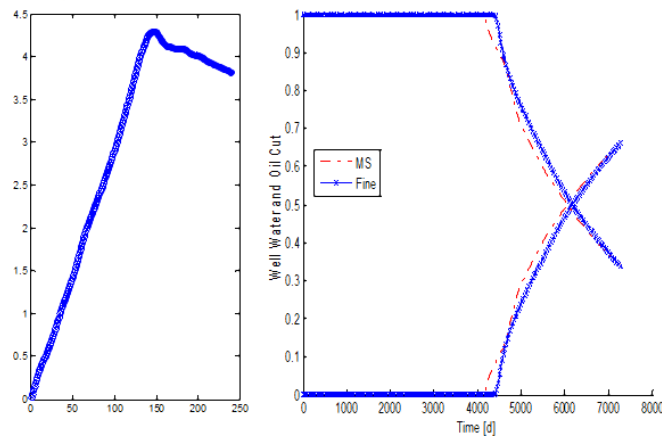


Figure 12. The left plot shows the percentage discrepancy between the saturation fields computed by the fine-scale and the multiscale simulations as a function of time step. The right plot shows the oil and water cuts as function of time.

the multiscale simulations, both in the saturation field and in the prediction of water breakthrough. Based on other experiments with the MsMFE method, we have reason to believe that improved accuracy can be observed if basis functions are updated throughout the simulation and the coarse partition is adapted somewhat to the variations in rock type.

4.5. Example 5: Compressible flow

In the last test, we consider a two-phase flow problem described by the compressible, black-oil equations. There are several ways to formulate and discretize this type of models; common for all successful approaches is that they rely on a meticulous choice of variables, linearizations, and averaging. A prerequisite for being able to formulate a successful, iterative MsMFE methodology is to have a robust numerical formulation for the fine-scale problem that solves the flow and transport sequentially in separate steps and relies on a mixed (hybrid) formulation of the flow equation. Several mixed methods are reported for the black-oil equations in the literature [38, 39, 40], but to the best of our knowledge, it is not yet clear that there exists such a formulation that is fully robust and efficient for black-oil models of industry-standard complexity. Herein, we will therefore use a sequential method with a straightforward mixed formulation for the pressure equation and

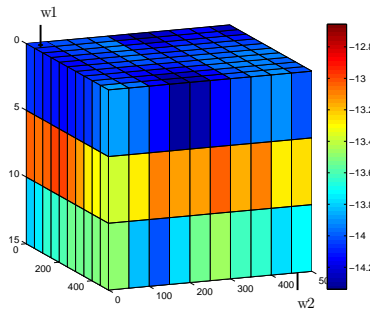


Figure 13. Well placement and permeability, plotted on \log_{10} -scale, for the compressible test case.

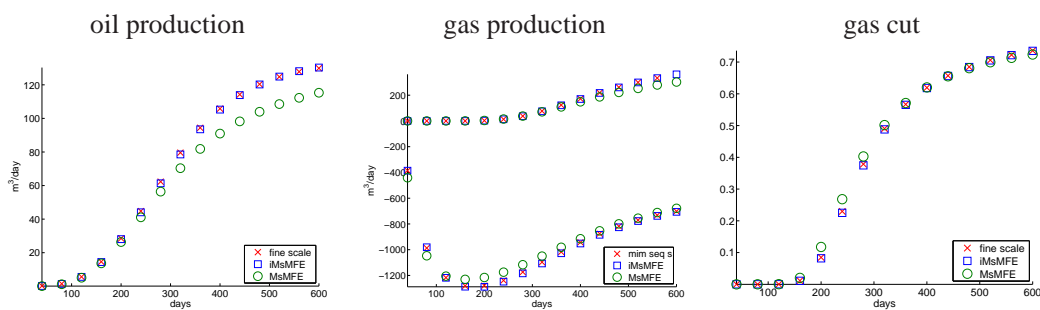


Figure 14. Oil production, gas production, and gas cut computed by the fine-scale and the multiscale solvers for a 3D compressible test case.

an implicit transport solver with saturation as primary variable, and simply assume that this is a reasonable solution strategy for the fine-scale equations.

We consider a sector of a reservoir in the shape of a $500 \times 500 \times 15m$ rectangular box, realized on a grid consisting of $10 \times 10 \times 3$ cells. The model is initially filled with oil at 200 bar. Gas is injected from a well located in one of the corners of the model and operating at a fixed bottom-hole pressure of 300 bar. Fluids are produced from a well located in the opposite corner, operating at a fixed bottom-hole pressure of 200 bar. Both fluids are assumed to be compressible, with a compressibility of $5 \cdot 10^{-3}$ bar for the oil, and the gas following an ideal gas law. The fluids have linear relative permeabilities and a viscosity of 1 cP for the oil and 0.1 cP for the gas. The heterogeneous permeability distribution and the well pattern are shown in Figure 13.

Our primary interest for this example is to investigate how well the MsMFE method predicts the global flow responses in this pressure-controlled system; that is, how accurate the method predicts oil and gas rates in the injector and producer, as well as the gas cut in the producer. To this end, we will compare a sequential, mixed-type, fine-scale solver with two different multiscale methods derived from the same fine-scale discretization, and working on a $5 \times 5 \times 1$ coarse grid. The first multiscale method is a straightforward extension of the original MsMFE method that uses a set of elliptic basis functions to compute the pressure. The second multiscale method is based on an iterative setup as discussed in Section 3.5. Figure 14 reports a comparison of oil production, gas production, and gas cut predicted by the three different methods. In the simulation, we have used equally spaced time steps, each of length 40 days, to reach the final time of 600 days. The original MsMFE method clearly underestimates the oil production, whereas the gas production and gas cut are calculated quite accurately. By adding extra iterations in the iMsMFE method, the multiscale method calculates a correct profile also for the oil production.

5. CONCLUSIONS

In this paper we have reviewed a multiscale mixed finite-element method for incompressible two-phase flow and discussed how to extend the method to include more realistic flow physics like gravity and spatially-dependent rock-fluid parameters. The method has been validated and benchmarked on a large number of test cases that focus on geological and petrophysical models with a high degree of realism, or on realistic flow physics on synthetic grid models designed to exemplify certain behavior. Selected results from four of these test cases were presented above. Altogether, these benchmark cases show that the MsMFE method is efficient, robust, and reasonably accurate compared to the fine-scale simulation and hence has a significant potential for accelerating simulation of two-phase flow applications, particularly for incompressible flow. Compared with coarse-scale models, the multiscale method gives a significant improvement of the accuracy and resolution of the flux, pressure, and saturation fields at a comparable computational cost. Combined with a large degree of robustness, this emphasizes the importance of the MsMFE method for its ability to capture fine-scale heterogeneity.

The MsMFE method can also be extended to compressible flow and has a certain potential both for weakly and strongly compressible problems, including black-oil models. Here, however, the formulation of an effective MsMFE method hinges on a crucial point: the fine-scale problem used as a starting point must be formulated in terms of a sequential solution procedure that contains a pressure equation discretized on mixed (hybrid) form. Although such discretizations can be formulated and good results can be obtained in many special cases, see e.g., [41, 42, 43, 44, 45], there is a need for more research to formulate a sequential fine-scale method that has the generality, robustness, and efficiency that is required if this method is to be applied for practical simulation of models of industry-standard complexity. If such a fine-scale formulation becomes available, our results along with results presented in [33] indicate that it will not be difficult to build an efficient MsMFE method on top of it.

REFERENCES

- Weinan E, Engquist B, Li X, Ren W, Vanden-Eijnden E. Heterogeneous multiscale methods: a review. *Communications in computational physics* 2007; **2**(3):367–450.
- Efendiev Y, Hou TY. *Multiscale Finite Element Methods, Surveys and Tutorials in the Applied Mathematical Sciences*, vol. 4. Springer Verlag, 2009.
- Guerillot D, Verdier S. Different pressure grids for reservoir simulation in heterogeneous reservoirs. *SPE Reservoir Simulation Symposium, 12-15 February 1995, San Antonio, Texas, USA*, 1995, doi:10.2118/29148-MS.
- Audigane P, Blunt MJ. Dual mesh method for upscaling in waterflood simulation. *Transp. Porous Media* 2004; **55**:71–89, doi:10.1023/B:TIPM.0000007309.48913.d2.
- Arbogast T. Implementation of a locally conservative numerical subgrid upscaling scheme for two-phase Darcy flow. *Comput. Geosci.* 2002; **6**(3-4):453–481, doi:10.1023/A:1021295215383.
- Arbogast T, Bryant SL. A two-scale numerical subgrid technique for waterflood simulations. *SPE J.* 2002; **7**(4):446–457, doi:10.2118/81909-PA.
- Hou TY, Wu XH. A multiscale finite element method for elliptic problems in composite materials and porous media. *J. Comput. Phys.* 1997; **134**(1):169–189, doi:10.1006/jcph.1997.5682.
- Chen A, Hou T. A mixed multiscale finite element method for elliptic problems with oscillating coefficients. *Math. Comp.* 2002; **72**(242):541–576, doi:10.1090/S0025-5718-02-01441-2.
- Aarnes JE. On the use of a mixed multiscale finite element method for greater flexibility and increased speed or improved accuracy in reservoir simulation. *Multiscale Model. Simul.* 2004; **2**(3):421–439, doi:10.1137/030600655.
- Aarnes JE, Krogstad S, Lie KA. Multiscale mixed/mimetic methods on corner-point grids. *Comput. Geosci.* 2008; **12**(3):297–315, doi:10.1007/s10596-007-9072-8.
- Alpak FO, Pal M, Lie KA. A multiscale method for modeling flow in stratigraphically complex reservoirs. *SPE J.* 2012; **17**(4):1056–1070, doi:10.2118/140403-PA.
- Jenny P, Lee SH, Tchelepi HA. Multi-scale finite-volume method for elliptic problems in subsurface flow simulation. *J. Comput. Phys.* 2003; **187**:47–67, doi:10.1016/S0021-9991(03)00075-5.
- Lee SH, Wolfsteiner C, Tchelepi H. Multiscale finite-volume formulation for multiphase flow in porous media: Black oil formulation of compressible, three phase flow with gravity. *Comput. Geosci.* 2008; **12**(3):351–366, doi:10.1007/s10596-007-9069-3.
- Hajibeygi H, Jenny P. Multiscale finite-volume method for parabolic problems arising from compressible multiphase flow in porous media. *J. Comput. Phys* 2009; **228**(14):5129 – 5147, doi:10.1016/j.jcp.2009.04.017.
- Hajibeygi H, Jenny P. Adaptive iterative multiscale finite volume method. *J. Comput. Phys* 2011; **230**(3):628 – 643, doi:10.1016/j.jcp.2010.10.009.

16. Møyner O, Lie KA. The multiscale finite-volume method on stratigraphic grids. *SPE J.* 2014; doi:10.2118/163649-PA.
17. Møyner O, Lie KA. A multiscale two-point flux-approximation method. *J. Comput. Phys.* 2014; .
18. Kippe V, Aarnes JE, Lie KA. A comparison of multiscale methods for elliptic problems in porous media flow. *Comput. Geosci.* 2008; **12**(3):377–398, doi:10.1007/s10596-007-9074-6.
19. Farmer CL. Upscaling: a review. *Int. J. Numer. Meth. Fluids* 2002; **40**(1–2):63–78, doi:10.1002/fld.267.
20. Durlafsky LJ. Upscaling and gridding of fine scale geological models for flow simulation 2005. Presented at 8th International Forum on Reservoir Simulation Iles Borromees, Stresa, Italy, June 20–24, 2005.
21. The MATLAB Reservoir Simulation Toolbox, version 2011b Jan 2012. <http://www.sintef.no/MRST/>.
22. Wheeler MF. Mimetic finite difference methods for flow in porous media. *Center for subsurface modeling industrial affiliates meeting, oct. 21–22*, University of Texas, Austin 2003.
23. Brezzi F, Lipnikov K, Simoncini V. A family of mimetic finite difference methods on polygonal and polyhedral meshes. *Math. Models Methods Appl. Sci.* 2005; **15**:1533–1553, doi:10.1142/S0218202505000832.
24. Brezzi F, Lipnikov K, Shashkov M, Simoncini V. A new discretization methodology for diffusion problems on generalized polyhedral meshes 2005. LAUR-05-8717, Report.
25. Aavatsmark I. An introduction to multipoint flux approximations for quadrilateral grids. *Comput. Geosci.* 2002; **6**:405–432, doi:10.1023/A:1021291114475.
26. Edwards MG, Rogers CF. Finite volume discretization with imposed flux continuity for the general tensor pressure equation. *Comput. Geosci.* 1998; **2**:259–290. 10.1023/A:1011510505406.
27. Pal M, Edwards MG, Lamb AR. Convergence study of a family of flux-continuous, finite-volume schemes for the general tensor pressure equation. *Internat. J. Numer. Methods Fluids* 2006; **51**(9-10):1177–1203, doi:10.1002/fld.1211.
28. Lamine S, Edwards MG. Higher order multidimensional wave oriented upwind schemes for flow in porous media on unstructured grids. *SPE Reservoir Simulation Symposium, The Woodlands, TX, USA, 2–4 February 2009*, 2009, doi:10.2118/119187-MS.
29. Lamine S, Edwards MG. Higher order multidimensional upwind convection schemes for flow in porous media on structured and unstructured quadrilateral grids. *SIAM J. Sci. Comput.* 2010; **32**(3):1119–1139, doi:10.1137/080727750.
30. Natvig JR, Skaflestad B, Bratvedt F, Bratvedt K, Lie KA, Laptev V, Khataniar SK. Multiscale mimetic solvers for efficient streamline simulation of fractured reservoirs. *SPE J.* 2011; **16**(4), doi:10.2118/119132-PA.
31. Lie KA, Natvig JR, Krogstad S, Yang Y, Wu XH. Grid adaptation for the Dirichlet–Neumann representation method and the multiscale mixed finite-element method. *Comput. Geosci.* 2014; doi:10.1007/s10596-013-9397-4.
32. Aarnes JE, Krogstad S, Lie KA. A hierarchical multiscale method for two-phase flow based upon mixed finite elements and nonuniform coarse grids. *Multiscale Model. Simul.* 2006; **5**(2):337–363, doi:10.1137/050634566.
33. Krogstad S, Lie KA, Skaflestad B. Mixed multiscale methods for compressible flow. *Proceedings of ECMOR XIII–13th European Conference on the Mathematics of Oil Recovery*, EAGE: Biarritz, France, 2012.
34. Krogstad S. A sparse basis POD for model reduction of multiphase compressible flow. *2011 SPE Reservoir Simulation Symposium, The Woodlands, Texas, USA, 21–23 February 2011*, 2011, doi:10.2118/141973-MS.
35. MoReS. Shell’s Reservoir Simulation Toolbox, version 2010. <http://www.shell.com> February 2010.
36. Lie K, Krogstad S, Ligaarden I, Natvig J, Nilsen H, Skaflestad B. Open-source MATLAB implementation of consistent discretisations on complex grids. *Comput. Geosci.* 2012; **16**:297–322. 10.1007/s10596-011-9244-4.
37. Notay Y. An aggregation-based algebraic multigrid method. *Electron. Trans. Numer. Anal.* 2010; **37**:123–140.
38. Bergamaschi L, Mantica S, Manzini G. A mixed finite element–finite volume formulation of the black-oil model. *SIAM Journal on Scientific Computing* 1998; **20**(3):970–997, doi:10.1137/S1064827595289303.
39. Chen Z. Formulations and numerical methods of the black oil model in porous media. *SIAM J. Numer. Anal.* Jul 2000; **38**(2):489–514, doi:10.1137/S0036142999304263.
40. Krogstad S, Lie KA, Nilsen HM, Natvig JR, Skaflestad B, Aarnes JE. A multiscale mixed finite-element solver for three-phase black-oil flow. *SPE Reservoir Simulation Symposium, The Woodlands, TX, USA, 2–4 February 2009*, 2009, doi:10.2118/118993-MS.
41. Bergamaschi L, Mantica S, Manzini G. A mixed finite element–finite volume formulation of the black-oil model. *SIAM J. Sci. Comput* 1998; **20**(3):970–997, doi:10.1137/S1064827595289303.
42. Chen Z. Formulations and numerical methods of the black oil model in porous media. *SIAM J. Numer. Anal.* 2000; **38**(2):489–514, doi:10.1137/S0036142999304263.
43. Yang D. A splitting positive definite mixed element method for miscible displacement of compressible flow in porous media. *Numer. Methods Partial Differential Equations* 2001; **17**(3):229–249, doi:10.1002/num.3.
44. Cui M. A combined mixed and discontinuous galerkin method for compressible miscible displacement problem in porous media. *J. Comput. Appl. Math.* 2007; **198**(1):19–34, doi:10.1016/j.cam.2005.11.021.
45. Yang Jm, Chen Y. Superconvergence of a combined mixed finite element and discontinuous Galerkin method for a compressible miscible displacement problem. *Acta Math. Appl. Sin.* 2011; **27**(3):481–494, doi:10.1007/s10255-011-0081-y.